Mathematical Modelling and Analysis
Volume 25, Issue 2, 208–225, 2020
https://doi.org/10.3846/mma.2020.9796

http://mma.vgtu.lt
ISSN: 1392-6292
eISSN: 1648-3510

A Quadratic C^0 Interior Penalty Method for the Quad-Curl Problem

Zhengjia Sun[a], Fuzheng Gao[b], Chao Wang[c] and Yi Zhang[d]

[a] *College of Economics, Shenzhen University*
Shenzhen, Guangdong 518060, China
[b] *School of Mathematics, Shandong University*
Jinan, Shandong 250100, China
[c] *Department of Applied Mathematics, The Hong Kong Polytechnic University*
Kowloon, Hong Kong, China
[d] *Department of Mathematics and Statistics, The University of North Carolina at Greensboro*
Greensboro, NC 27402, USA
E-mail: sunzhengjia@szu.edu.cn
E-mail: fzgao@sdu.edu.cn
E-mail(*corresp.*): chao.qa.wang@connect.polyu.hk
E-mail: y_zhang7@uncg.edu

Received March 29, 2019; revised January 13, 2020; accepted January 14, 2020

Abstract. In this paper we study the C^0 interior penalty method for a quad-curl problem arising from magnetohydrodynamics model on bounded polygons or polyhedrons. We prove the well-posedness of the numerical scheme and then derive the optimal error estimates in a discrete energy norm. A post-processing procedure that can produce C^1 approximations is also presented. The performance of the method is illustrated by numerical experiments.

Keywords: C^0 interior penalty method, MHD, quad-curl problem, error analysis.

AMS Subject Classification: 65N15; 65N30.

1 Introduction

The magnetohydrodynamics (MHD) model [1, 11] has wide range of applications in plasma physics, astrophysics, magnetospheric and thermonuclear fusion. It describes the motion of electrical conducting fluid in the presence of a

magnetic field. In the MHD model, the behavior of a continuous fluid is governed by a simplified form of Maxwell's equation, together with Ohm's law and Navier-Stokes equations. The MHD system with hyper-resistivity is described as follows:

$$\begin{cases} \rho(\boldsymbol{u}_t + \boldsymbol{u}\cdot\nabla\boldsymbol{u}) + \nabla p = \dfrac{1}{\mu_0}(\nabla\times\mathbf{B})\times\mathbf{B} + \mu\Delta\boldsymbol{u}, \\ \nabla\cdot\boldsymbol{u} = 0, \\ \mathbf{B}_t - \nabla\times(\boldsymbol{u}\times\mathbf{B}) = -\dfrac{\eta_1}{\mu_0}(\nabla\times)^2\mathbf{B} - \dfrac{d_i}{\mu_0}\nabla\times((\nabla\times\mathbf{B})\times\mathbf{B}) - \dfrac{\eta_2}{\mu_0}(\nabla\times)^4\mathbf{B}, \\ \nabla\cdot\mathbf{B} = 0, \end{cases}$$

where $\boldsymbol{u}$ is the fluid velocity, $\mathbf{B}$ is the magnetic field, ρ is the density, p is the static pressure, η_1 is the resistivity, η_2 is the hyper-resistivity, μ_0 is the magnetic permeability of free space, μ is the viscosity, and d_i is the ion inertial length.

When simulating the MHD system, the velocity $\boldsymbol{u}$ and pressure p are often discretized by using the standard finite element method. However, for the magnetic field variable $\mathbf{B}$, such approach will encounter difficulties because of the existence of the fourth order term $(\nabla\times)^4\mathbf{B}$. In particular, an H^2-conforming method would have 220 degrees of freedom per element to approximate the solutions. Hence it is more practical to use the nonconforming finite element method [26] or mixed finite element method [20] to solve the above quad-curl model problem. However, other problems may arise. More precisely, though the number of degree of freedom can be greatly reduced by using nonconforming and mixed finite element methods, the implementations of Morley-type elements [14,16] and high order Nédélec's edge elements [17,18] are more challenging than the simple standard P_k Lagrange finite elements. Moreover, the error analysis for nonconforming and mixed methods is more complicated. The MHD model problem was also solved by the discontinuous Galerkin (DG) method [13] using weakly $H(\mathrm{curl})$-conforming elements. Recently, Brenner et al. [5] studied the P_k Lagrange finite element methods for the quad-curl problem based on the Hodge decomposition for divergence-free vector fields. Their idea is to decompose the two-dimensional model vector problem into a sequence of second order elliptic scalar problems, which makes the two-dimensional problem easier to be solved by standard conforming FEM. Recently, Zhang et al. [24] developed an $H^2(\mathrm{curl})$-conforming finite element in two dimensions and applied it to solve the quad-curl model problem. Chen et al. [12] proposed a mixed finite element method for a problem with a quad-curl term. In this work, they also used the standard P_k Lagrange finite element to approximate the variables. However, the stability requires the inf-sup condition, which is a complicated process. This analysis was obtained by using the discrete Sobolev embedding inequalities for the piecewise polynomials.

In this work, we focus on the following three dimensional quad-curl model problem which is deduced from the magnetic induction equations in the MHD model [26]. Let Ω be a bounded polyhedral domain in $\mathbb{R}^3$ and $\boldsymbol{f}\in[L_2(\Omega)]^3$.

We consider the model problem

$$\begin{cases} (\nabla\times)^4\boldsymbol{u}+\beta\,\nabla\times\nabla\times\boldsymbol{u}+\gamma\,\boldsymbol{u}=\boldsymbol{f} & \text{in } \Omega,\\ \nabla\cdot\boldsymbol{u}=0 & \text{in } \Omega,\\ \boldsymbol{u}\times\boldsymbol{n}=0,\quad \nabla\times\boldsymbol{u}=0 & \text{on } \partial\Omega, \end{cases} \tag{1.1}$$

where $(\nabla\times)^4=(\nabla\times\nabla\times\nabla\times\nabla\times)$, β and γ are nonnegative constants, and $\gamma>0$ if Ω is not simply connected. The quad-curl model problem (1.1) also appears in the Maxwell's transmission problem [15] and the inverse electromagnetic scattering theory [9, 10]. The weak problem of (1.1) is as follows: find $\boldsymbol{u}\in\mathbb{E}$ such that

$$a(\boldsymbol{u},\boldsymbol{v})=(\boldsymbol{f},\boldsymbol{v}),\quad \forall\,\boldsymbol{v}\in\mathbb{E}, \tag{1.2}$$

where

$$a(\boldsymbol{u},\boldsymbol{v})=\big(\nabla\times\nabla\times\boldsymbol{u},\nabla\times\nabla\times\boldsymbol{v}\big)+\beta(\nabla\times\boldsymbol{u},\nabla\times\boldsymbol{v})+\gamma(\boldsymbol{u},\boldsymbol{v}), \tag{1.3}$$

$$\mathbb{E}=\big\{\boldsymbol{v}\in[L_2(\Omega)]^3:\nabla\times\,\boldsymbol{v}\in[H_0^1(\Omega)]^3,\ \nabla\cdot v{=}0 \text{ in } \Omega, \text{ and } \boldsymbol{n}\times\boldsymbol{v}{=}0 \text{ on } \partial\Omega\big\}.$$

As the functions in $\mathbb{E}$ are divergence-free, it is easy to show that equation (1.2) is elliptic. Thus Lax-Milgram theory indicates that the problem (1.2) is well-posed [5]. The regularity of the quad-curl model problem (1.1)–(1.2) on general polyhedral domains is still unknown. The most recent results on the regularity of the solution of (1.1)–(1.2) are as follows. On convex polyhedral domains, it was proved in [25] that $\boldsymbol{u}\in[H^2(\Omega)]^3$ and $\nabla\times\boldsymbol{u}\in[H^2(\Omega)]^3$, in the case where $\nabla\cdot\boldsymbol{f}=0$. However, in [19] S. Nicaise showed that $\boldsymbol{u}\notin[H^2(\Omega)]^3$ on general polyhedral domains. In particular, when $\nabla\cdot\boldsymbol{f}=0$, both the solution $\boldsymbol{u}$ and $\nabla\times\boldsymbol{u}$ belong to $[H^{\frac{1}{2}+\delta}(\Omega)]^3$ for some $\delta\in(0,\frac{1}{2}]$. Due to the lack of regularity results, the nonconforming finite element method in [26] was introduced and studied for the model problem (1.2), assuming that $\boldsymbol{u}\in[H^4(\Omega)]^3$. In [13], a discontinuous Galerkin method for the quad-curl problem was studied under the assumption that $\boldsymbol{u}\in[H^2(\Omega)]^3$ and $\nabla\times\boldsymbol{u}\in[H^2(\Omega)]^3$. The mixed finite element method in [20] for the quad-curl eigenvalue problem was analyzed under the assumption that $(\nabla\times)^j\boldsymbol{u}\in[L_2(\Omega)]^3$, $j=0,1,2,3$. In [12], the regularity results for non-convex Lipschitz polyhedral domains in three dimensions was proved. It is shown therein $\boldsymbol{u}\in[H^\alpha(\Omega)]^3$ and $\nabla\times\boldsymbol{u}\in[H^\beta(\Omega)]^3$, where $\alpha\in(1/2,1]$ and $\beta\in[1,3/2)$. The mixed finite element method was studied, under a lower assumption that $\boldsymbol{u}\in[H^{r_1}(\Omega)]^3$, $\nabla\times\boldsymbol{u}\in[H^{r_2}(\Omega)]^3$, and $\nabla\times\nabla\times\boldsymbol{u}\in[H^{r_3}(\Omega)]^3$, where $r_1\in(1/2,\infty)$, $r_2\in[1,\infty)$ and $r_3\in(3/2,\infty)$.

In this paper, we consider the C^0 interior penalty (C^0-IP) method [2, 6] to solve the quad-curl problem (1.2). One major merit of the C^0-IP method is that it uses lower order P_k polynomials, which is much simpler than C^1-conforming and curl-curl conforming finite element methods. Therefore, both the construction of the finite element space and the error analysis of the C^0-IP method are straightforward. Moreover, the positive definiteness of the continuous problem can also be preserved by the numerical scheme even for more complicated elliptic systems. On the other hand, for the C^0-IP method, there is no need to

include penalization terms involving the jumps of discrete functions. Hence the computational cost is considerably less than for the conventional DG methods. These advantages make C^0-IP method more attractive for solving fourth order problems [8]. Furthermore, the C^0-IP scheme for lower order elliptic problems can be exploited in the design of an effective smoother for fast solvers, such as multigrid algorithms for higher order problems [7, 21].

The rest of this paper is organized as follows. In Section 2, we introduce the C^0 interior penalty method for (1.2) and prove the well-posedness of the numerical scheme. In Section 3, we derive optimal error estimates in a discrete energy norm. A post-processing procedure which further produces C^1 approximations is also studied. Several numerical experiments are carried out to illustrate the performance of the numerical scheme. The results are reported in Section 4.

For convenience, we will use the notation $A \lesssim B$ throughout the paper to represent the inequality $A \leq \text{Constant} \times B$, where the constant, unless otherwise specified, depends only on the shape regularity (or equivalently the minimum angle) of $\mathcal{T}_h$. The statement $A \approx B$ is equivalent to $A \lesssim B$ and $B \lesssim A$.

2 The C^0 interior penalty method

2.1 Preliminaries

Let $\mathcal{T}_h$ be a regular tetrahedron mesh of $\Omega \in \mathbb{R}^3$. The diameter of a tetrahedron $T \in \mathcal{T}_h$ is denoted by h_T. The mesh parameter $h = \max_{T\in\mathcal{T}_h} h_T$. We denote the set of faces of the tetrahedrons in $\mathcal{T}_h$ by $\mathcal{F}_h = \mathcal{F}_h^i \cup \mathcal{F}_h^b$, where $\mathcal{F}_h^i$ is the set of the interior faces and $\mathcal{F}_h^b$ is the set of the faces on $\partial\Omega$. Define the piecewise Sobolev space as

$$H^s(\Omega, \mathcal{T}_h) = \big\{\boldsymbol{v} \in [L_2(\Omega)]^3 : \boldsymbol{v}_T \in [H^s(T)]^3, \quad \forall\, T \in \mathcal{T}_h\big\},$$

where $\boldsymbol{v}_T = \boldsymbol{v}\big|_T$.

The construction of the quadratic C^0 interior penalty method requires the concepts of jumps and average of functions across the element interfaces $\mathcal{F}_h$, which are defined below.

Let $F \in \mathcal{F}_h^i$ be an interior face shared by two tetrahedrons T_- and T_+, and $\boldsymbol{n}_e$ be the unit normal of F pointing from T_- to T_+. We define on F

$$\{\!\{\nabla\times\nabla\times\boldsymbol{v}\}\!\} = \frac{1}{2}\big(\nabla\times\nabla\times\boldsymbol{v}_- + \nabla\times\nabla\times\boldsymbol{v}_+\big), \quad \forall\,\boldsymbol{v} \in H^s(\Omega,\mathcal{T}_h),\ s > \frac{5}{2},$$
$$[\![\nabla\times\boldsymbol{v}]\!] = (\nabla\times\boldsymbol{v}_-)\times\boldsymbol{n}_e - (\nabla\times\boldsymbol{v}_+)\times\boldsymbol{n}_e, \qquad \forall\,\boldsymbol{v} \in H^2(\Omega,\mathcal{T}_h),$$

where $\boldsymbol{v}_\pm = \boldsymbol{v}\big|_{T_\pm}$. On $F \in \mathcal{F}_h^b$, we take $\boldsymbol{n}_e$ to be the unit normal of F that points towards the outside of Ω and define

$$\{\!\{\nabla\times\nabla\times\boldsymbol{v}\}\!\} = \nabla\times\nabla\times\boldsymbol{v}_T, \quad \forall\,\boldsymbol{v} \in H^s(\Omega,\mathcal{T}_h),\ s > 2.5,$$
$$[\![\nabla\times\boldsymbol{v}]\!] = (\nabla\times\boldsymbol{v}_T)\times\boldsymbol{n}_e, \quad \forall\,\boldsymbol{v} \in H^2(\Omega,\mathcal{T}_h).$$

Remark 1. Note that in $\mathbb{R}^2$, $\nabla \times \boldsymbol{v}$ is a scalar function. Hence the average terms are defined as the same formulation as in three dimension. However, the jump terms are defined to be vector functions as below.

$$[\![\nabla \times \boldsymbol{v}]\!] = (\nabla \times \boldsymbol{v}_-)\boldsymbol{t}_e - (\nabla \times \boldsymbol{v}_+)\boldsymbol{t}_e, \ \ \forall\, \boldsymbol{v} \in H^2(\Omega, \mathcal{T}_h) \text{ on the interior edge},$$
$$[\![\nabla \times \boldsymbol{v}]\!] = (\nabla \times \boldsymbol{v}_T)\boldsymbol{t}_e, \qquad \forall\, \boldsymbol{v} \in H^2(\Omega, \mathcal{T}_h) \quad \text{on the boundary edge},$$

where $\boldsymbol{t}_e$ is the unit tangent vector which is obtained by rotating $\boldsymbol{n}_e$ by a right-angle clockwisely.

2.2 The discrete problem

Let $V_h(\subset [H^1(\Omega)]^3)$ be the P_2-vector Lagrange finite element space associated with $\mathcal{T}_h$, such that the tangential components of its members vanish on all nodal points on the boundary of Ω. More precisely,

$$V_h = \{\boldsymbol{v} \in [H^1(\Omega)]^3 : \boldsymbol{v}_T \in [P_2(T)]^3,$$
$$\boldsymbol{n} \times \boldsymbol{v}_T = 0 \text{ on the vertices and midpoints of each edge of } F \in \mathcal{F}_h^b\}.$$

Let $\boldsymbol{u}$ be the solution of the quad-curl problem (1.1) and $\boldsymbol{v} \in [P_2(T)]^3$. We assume that $\boldsymbol{u} \in [H^{2+\alpha}(\Omega)]^3$ so that the construction of the discrete scheme makes sense. For any $T \in \mathcal{T}_h$, by using Green's formula we have

$$\begin{aligned}\int_T \boldsymbol{f} \cdot \boldsymbol{v}\, dx = &\int_T (\nabla \times \nabla \times \boldsymbol{u}) \cdot (\nabla \times \nabla \times \boldsymbol{v})\, dx + \beta \int_T (\nabla \times \boldsymbol{u}) \cdot (\nabla \times \boldsymbol{v})\, dx \\ &+ \gamma \int_T \boldsymbol{u} \cdot \boldsymbol{v}\, dx + \int_{\partial T} (\nabla \times \nabla \times \boldsymbol{u}) \cdot (\nabla \times \boldsymbol{v}) \times \boldsymbol{n}\, ds \\ &+ \int_{\partial T} (\nabla \times)^3 \boldsymbol{u} \cdot \boldsymbol{v} \times \boldsymbol{n}\, ds + \int_{\partial T} \nabla \times \boldsymbol{u} \cdot \boldsymbol{v} \times \boldsymbol{n}\, ds.\end{aligned} \tag{2.1}$$

By summing up (2.1) over all $T \in \mathcal{T}_h$ and considering the definition V_h, we find

$$\begin{aligned}&\sum_{T \in \mathcal{T}_h} \int_T (\nabla \times \nabla \times \boldsymbol{u}) \cdot (\nabla \times \nabla \times \boldsymbol{v})\, dx + \beta \sum_{T \in \mathcal{T}_h} \int_T (\nabla \times \boldsymbol{u}) \cdot (\nabla \times \boldsymbol{v})\, dx \\ &\quad + \gamma \sum_{T \in \mathcal{T}_h} \int_T \boldsymbol{u} \cdot \boldsymbol{v}\, dx + \sum_{F \in \mathcal{F}_h} \int_F \{\!\{\nabla \times \nabla \times \boldsymbol{u}\}\!\} \cdot [\![\nabla \times \boldsymbol{v}]\!]\, ds = \int_T \boldsymbol{f} \cdot \boldsymbol{v}\, dx\end{aligned} \tag{2.2}$$

for all $\boldsymbol{v} \in V_h$. Since $[\![\nabla \times \boldsymbol{u}]\!] = 0$ for all $F \in \mathcal{F}_h$, we can rewrite (2.2) as

$$\begin{aligned}&\sum_{T \in \mathcal{T}_h} \int_T (\nabla \times \nabla \times \boldsymbol{u}) \cdot (\nabla \times \nabla \times \boldsymbol{v})\, dx + \beta \sum_{T \in \mathcal{T}_h} \int_T (\nabla \times \boldsymbol{u}) \cdot (\nabla \times \boldsymbol{v})\, dx \\ &+ \gamma \sum_{T \in \mathcal{T}_h} \int_T \boldsymbol{u} \cdot \boldsymbol{v}\, dx + \sum_{F \in \mathcal{F}_h} \int_F \{\!\{\nabla \times \nabla \times \boldsymbol{u}\}\!\} \cdot [\![\nabla \times \boldsymbol{v}]\!]\, ds \\ &+ \sum_{F \in \mathcal{F}_h} \int_F \{\!\{\nabla \times \nabla \times \boldsymbol{v}\}\!\} \cdot [\![\nabla \times \boldsymbol{u}]\!]\, ds + \sum_{F \in \mathcal{F}_h} \frac{\sigma}{|e|} \int_F [\![\nabla \times \boldsymbol{u}]\!] \cdot [\![\nabla \times \boldsymbol{v}]\!]\, dx \\ &= \int_T \boldsymbol{f} \cdot \boldsymbol{v}\, dx, \quad \forall\, \boldsymbol{v} \in V_h,\end{aligned}$$

where $|e|$ is the diameter of the face F, and $\sigma > 0$ is the penalty parameter to be chosen later.

The C^0 interior penalty method for the quad-curl problem (1.2) is defined as follows: find $\boldsymbol{u}_h \in V_h$ such that

$$a_h(\boldsymbol{u}_h, \boldsymbol{v}) = (\boldsymbol{f}, \boldsymbol{v}), \qquad \forall\ \boldsymbol{v} \in V_h, \tag{2.3}$$

where

$$\begin{aligned} a_h(\boldsymbol{u}, \boldsymbol{w}) &= \sum_{T\in\mathcal{T}_h} \int_T (\nabla\times\nabla\times\boldsymbol{u})\cdot(\nabla\times\nabla\times\boldsymbol{w})\,dx \\ &+ \beta \sum_{T\in\mathcal{T}_h} \int_T (\nabla\times\boldsymbol{u})\cdot(\nabla\times\boldsymbol{w})\,dx + \sum_{F\in\mathcal{F}_h} \int_F \{\!\{\nabla\times\nabla\times\boldsymbol{u}\}\!\}\cdot[\![\nabla\times\boldsymbol{w}]\!]\,ds \\ &+ \gamma \sum_{T\in\mathcal{T}_h} \int_T \boldsymbol{u}\cdot\boldsymbol{w}\,dx + \sum_{F\in\mathcal{F}_h} \int_F \{\!\{\nabla\times\nabla\times\boldsymbol{w}\}\!\}\cdot[\![\nabla\times\boldsymbol{u}]\!]\,ds \\ &+ \sum_{F\in\mathcal{F}_h} \frac{\sigma}{|e|} \int_F [\![\nabla\times\boldsymbol{u}]\!]\cdot[\![\nabla\times\boldsymbol{w}]\!]\,ds + \sum_{T\in\mathcal{T}_h} \frac{1}{h_T^2} \int_T (\nabla\cdot\boldsymbol{u})(\nabla\cdot\boldsymbol{w})\,dx. \end{aligned} \tag{2.4}$$

Remark 2. The first four terms on the right-hand side of (2.4) come from integration by parts. The fifth term is added for symmetry. The sixth term is the penalization term (with penalty parameter $\sigma > 0$). In the analysis of well-posedness, the penalty parameter σ is chosen to be large enough in order to derive the coercivity of the discrete bilinear form $a_h(\cdot,\cdot)$. The last term is added to the numerical scheme to (weakly) enforce the divergence-free condition for the discrete solution. The inclusion of this term provides a good approximation of divergence free condition. We can also remove this term from the discrete scheme by adding a locally divergence free condition in the discrete space V_h. However, such approach will make the construction of V_h more complicated.

2.3 Well-posedness of the discrete problem

Lemma 1 [Consistency]. *For $\boldsymbol{f} \in [L_2(\Omega)]^3$, it is obvious that the solution $\boldsymbol{u}$ of* (1.2) *satisfies*

$$a_h(\boldsymbol{u}, \boldsymbol{v}) = (\boldsymbol{f}, \boldsymbol{v}), \qquad \forall\, \boldsymbol{v}\ \in\ V_h.$$

It follows from (2.3) and Lemma 1 that the following Galerkin orthogonality holds

$$a_h(\boldsymbol{u} - \boldsymbol{u}_h, \boldsymbol{v}) = 0, \qquad \forall\, \boldsymbol{v}\ \in\ V_h. \tag{2.5}$$

Define the discrete energy norm as

$$\begin{aligned} \|\boldsymbol{v}\|_h^2 &= \sum_{T\in\mathcal{T}_h} \|\nabla\times\nabla\times\boldsymbol{v}\|_{L^2(T)}^2 + \sum_{T\in\mathcal{T}_h} \|\nabla\times\boldsymbol{v}\|_{L^2(T)}^2 + \sum_{T\in\mathcal{T}_h} \|\boldsymbol{v}\|_{L^2(T)}^2 \\ &+ \sum_{F\in\mathcal{F}_h} \frac{1}{|e|} \|[\![\nabla\times\boldsymbol{v}]\!]\|_{L^2(F)}^2 + \sum_{F\in\mathcal{F}_h} |e| \|\{\!\{\nabla\times\nabla\times\boldsymbol{v}\}\!\}\|_{L^2(F)}^2 \\ &+ \sum_{T\in\mathcal{T}_h} \frac{1}{h_T^2} \|\nabla\cdot\boldsymbol{v}\|_{L^2(T)}^2. \end{aligned} \tag{2.6}$$

Lemma 2 [Continuity]. *It is easy to show that the bilinear form $a_h(\cdot,\cdot)$ is bounded in the sense that*

$$|a_h(\boldsymbol{u},\boldsymbol{w})| \leq C\|\boldsymbol{u}\|_h\|\boldsymbol{w}\|_h, \quad \forall\, \boldsymbol{u},\boldsymbol{w} \in [H^{2+\alpha}(\Omega)]^3 + V_h, \tag{2.7}$$

for any $\alpha > \frac{1}{2}$, where $C = max(\|\beta\|_{L^\infty(\Omega)}, \|\gamma\|_{L^\infty(\Omega)}, 1+\sigma)$.

Lemma 3 [Norm-equivalence]. *There exists a positive constant C_1 depending only on the shape regularity of $\mathcal{T}_h$ such that*

$$|\!|\!|\boldsymbol{v}|\!|\!|_{H^2(\Omega,\mathcal{T}_h)} \leq \|\boldsymbol{v}\|_h \leq C_1|\!|\!|\boldsymbol{v}|\!|\!|_{H^2(\Omega,\mathcal{T}_h)}, \qquad \forall\, \boldsymbol{v} \in V_h, \tag{2.8}$$

where the seminorm $|\!|\!|\cdot|\!|\!|_{H^2(\Omega,\mathcal{T}_h)}$ is defined by

$$\begin{aligned} |\!|\!|\boldsymbol{v}|\!|\!|^2_{H^2(\Omega,\mathcal{T}_h)} = &\sum_{T\in\mathcal{T}_h} \|\nabla\times\nabla\times\boldsymbol{v}\|^2_{L^2(T)} + \sum_{T\in\mathcal{T}_h}\|\boldsymbol{v}\|^2_{L^2(T)} \\ &+ \sum_{F\in\mathcal{F}_h}\frac{1}{|e|}\|[\![\nabla\times\boldsymbol{v}]\!]\|^2_{L^2(F)} + \sum_{T\in\mathcal{T}_h}\frac{1}{h_T^2}\|\nabla\cdot\boldsymbol{v}\|^2_{L^2(T)}. \end{aligned} \tag{2.9}$$

Proof. The first inequality in (2.8) is obvious by (2.6) and (2.9).
By the trace theorem(with scaling) and standard inverse estimates, we have

$$\sum_{F\in\mathcal{F}_h}|e|\|\{\!\{\nabla\times\nabla\times\boldsymbol{v}\}\!\}\|^2_{L^2(F)} \lesssim \sum_{T\in\mathcal{T}_h}\|\nabla\times\nabla\times\boldsymbol{v}\|^2_{L^2(T)}. \tag{2.10}$$

Moreover, it follows from Poincare-Friedrichs inequality (cf. [4]) for piecewise H^1 functions that

$$\begin{aligned} \sum_{T\in\mathcal{T}_h}\|\nabla\times\boldsymbol{v}\|^2_{L^2(T)} \lesssim &\sum_{T\in\mathcal{T}_h}\|\nabla\times\nabla\times\boldsymbol{v}\|^2_{L^2(T)} + \sum_{T\in\mathcal{T}_h}\|\boldsymbol{v}\|^2_{L^2(T)} \\ &+ \sum_{F\in\mathcal{F}_h}|e|^{-1}\|[\![\nabla\times\boldsymbol{v}]\!]\|^2_{L^2(F)}. \end{aligned} \tag{2.11}$$

The second inequality in (2.8) now follows from (2.6), (2.9), (2.10) and (2.11). □

Lemma 4 [Coercivity]. *When the penalty parameter σ is chosen to be sufficiently large, there exists a constant C_* such that*

$$a_h(\boldsymbol{v},\boldsymbol{v}) \geq C_*\|\boldsymbol{v}\|^2_h, \qquad \forall\, \boldsymbol{v} \in V_h. \tag{2.12}$$

Proof. By Cauchy-Schwarz inequality and (2.10), we have

$$\begin{aligned} &\sum_{F\in\mathcal{F}_h}\left|\int_F \{\!\{\nabla\times\nabla\times\boldsymbol{v}\}\!\}\cdot[\![\nabla\times\boldsymbol{v}]\!]\,ds\right| \\ &\leq \sum_{F\in\mathcal{F}_h}\left[(\epsilon|e|)\|\{\!\{\nabla\times\nabla\times\boldsymbol{v}\}\!\}\|^2_{L^2(F)} + (\epsilon^{-1}|e|^{-1})\|[\![\nabla\times\boldsymbol{v}]\!]\|^2_{L^2(F)}\right] \\ &\leq C_2\epsilon\sum_{T\in\mathcal{T}_h}\|\nabla\times\nabla\times\boldsymbol{v}\|^2_{L^2(T)} + \epsilon^{-1}\sum_{F\in\mathcal{F}_h}|e|^{-1}\|[\![\nabla\times\boldsymbol{v}]\!]\|^2_{L^2(F)}, \end{aligned}$$

for all $\boldsymbol{v} \in V_h$, where $\epsilon > 0$ is arbitrary and $C_2 > 0$ depends only on the shape regularity of $\mathcal{T}_h$. By choosing $\epsilon = \frac{1}{2C_2}$, $\sigma = \frac{1}{2} + \frac{1}{\epsilon}$, and in view of (2.4), (2.8) and (2.9), we get

$$\frac{1}{2C_1}\|\boldsymbol{v}\|_h^2 \leq \frac{1}{2}|\!|\!|\boldsymbol{v}|\!|\!|^2_{H^2(\Omega,\mathcal{T}_h)} \leq a_h(\boldsymbol{v},\boldsymbol{v}), \qquad \forall\, \boldsymbol{v} \in V_h.$$

□

Combining Lemma 1, Lemma 2 and Lemma 4, the discrete problem (2.3) is well-posed under the assumptions of Lemma 4.

2.4 Enriching operator

In this subsection, we introduce an enriching operator which will be used later to construct a post-processing procedure that produces a C^1 approximation solution. The enriching operator measures the distance between V_h and the Sobolev space $[H^2(\Omega)]^3$: $E_h : V_h \to [H^2(\Omega)]^3$. The construction of E_h uses the C^1-Ženíšek finite element space (cf. [22]).

We briefly introduce the idea as follows. More details can be found in [6]. Let P_i, P_j, P_k, P_l be the four vertices of the tetrahedron T, $Q_{jk}^{(1,s)}, ..., Q_{jk}^{(s,s)}$ be the points dividing the edge P_jP_k into $s+1$ equal parts, Q_i be the triangular face which lies opposite to the vertex P_i, P_0 be the center of gravity of the tetrahedron T, as shown in Figure 1.

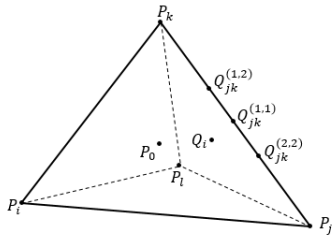

Figure 1. Nodal points for C^1-Ženíšek finite element.

For any $\boldsymbol{v} \in V_h$, we define $\boldsymbol{w} = E_h\boldsymbol{v}$ by averaging. More precisely, at the interior vertices P of $\mathcal{T}_h$, we take

$$\boldsymbol{w}(P) = \boldsymbol{v}(P), \tag{2.13}$$

$$\nabla \cdot \boldsymbol{w}(P) = \frac{1}{|\mathcal{T}_p|}\sum_{T\in\mathcal{T}_p}(\nabla\cdot\boldsymbol{v}_T)(P), \tag{2.14}$$

$$(\nabla\times\nabla\times\boldsymbol{w})(P) = \frac{1}{|\mathcal{T}_p|}\sum_{T\in\mathcal{T}_p}(\nabla\times\nabla\times\boldsymbol{v}_T)(P), \tag{2.15}$$

where $\mathcal{T}_p$ is the set of tetrahedrons in $\mathcal{T}_h$ whose closures share the nodal point P.

At the points on edges, we take

$$D^{\beta}_{jk}w^m(Q^{(r,s)}_{jk}) = \frac{1}{|\mathcal{T}_p|}\sum_{T\in\mathcal{T}_Q} D^{\beta}_{jk}v^m_T(Q^{(r,s)}_{jk}),\ \ |\beta| = s,\ r = 1, ..., s, .$$

$s = 1, 2, m = 1, 2, 3$. At the center of gravity Q of the triangular face, we take

$$\boldsymbol{w}(Q) = \boldsymbol{v}(Q),\ \ (\nabla\times\boldsymbol{w}\times\boldsymbol{n})(Q) = \frac{1}{|\mathcal{T}_Q|}\sum_{T\in\mathcal{T}_Q}(\nabla\times\boldsymbol{v}_T\times\boldsymbol{n})(Q),$$

$$(\nabla\times\nabla\times\boldsymbol{w}\times\boldsymbol{n})(Q) = \frac{1}{|\mathcal{T}_Q|}\sum_{T\in\mathcal{T}_Q}(\nabla\times\nabla\times\boldsymbol{v}_T\times\boldsymbol{n})(Q). \tag{2.16}$$

At the center of gravity P_0 of the tetrahedron, we take

$$\boldsymbol{w}(P_0) = \boldsymbol{v}(P_0)\quad\text{and}\quad(\nabla\times\boldsymbol{w})(P_0) = (\nabla\times\boldsymbol{v})(P_0). \tag{2.17}$$

Lemma 5. *It holds that*

$$\|\boldsymbol{v} - E_h\boldsymbol{v}\|_{L^2(\Omega)} \lesssim h^2|\!|\!|\boldsymbol{v}|\!|\!|_{H^2(\Omega,\mathcal{T}_h)},\qquad \forall\,\boldsymbol{v}\in V_h, \tag{2.18}$$

$$|E_h\boldsymbol{v}|_{H^2(\Omega)} \lesssim |\!|\!|\boldsymbol{v}|\!|\!|_{H^2(\Omega,\mathcal{T}_h)},\qquad \forall\,\boldsymbol{v}\in V_h. \tag{2.19}$$

Proof. Let $T\in\mathcal{T}_h$ be arbitrary and $\mathcal{N}(T)$ be the set of nodal variables of the C^1-Ženíšek finite element. It follows from (2.13), (2.16), (2.17) and scaling that

$$\|\boldsymbol{v} - E_h\boldsymbol{v}\|^2_{L^2(T)} \approx\ h_T^6\sum_{P\in\mathcal{M}_T}|\nabla\times\nabla\times(\boldsymbol{v}_T - E_h\boldsymbol{v})(P)|^2 + h_T^4\sum_{P\in\mathcal{V}_T}$$
$$\times|\nabla\cdot(\boldsymbol{v} - E_h\boldsymbol{v})(P)|^2 + h_T^4\sum_{P\in\mathcal{M}_T}|\nabla\times(\boldsymbol{v}\times\boldsymbol{n} - E_h\boldsymbol{v}\times\boldsymbol{n})(P)|^2. \tag{2.20}$$

Here $\mathcal{V}_T$ is the set of the four vertices of T and $\mathcal{M}_T$ is the set of the centers of gravity of the triangular faces. From (2.15) we have

$$\nabla\times\nabla\times(\boldsymbol{v}_T - E_h\boldsymbol{v})(P) = \frac{1}{|\mathcal{T}_p|}\sum_{T'\in\mathcal{T}_P}\nabla\times\nabla\times(\boldsymbol{v}_{T'} - \boldsymbol{v}_T)(P).$$

It then follows from scaling that

$$\sum_{P\in\mathcal{V}_T}|\nabla\times\nabla\times(\boldsymbol{v}_T - E_h\boldsymbol{v})(P)|^2 \lesssim \sum_{T'\in\mathcal{T}_p}h_{T'}^{-2}\|\nabla\times\nabla\times\boldsymbol{v}_{T'}\|^2_{L^2(T')}. \tag{2.21}$$

Similarly, by using (2.14) we have

$$\nabla\cdot(\boldsymbol{v}_T - E_h\boldsymbol{v})(P) = \frac{1}{|\mathcal{T}_p|}\sum_{T'\in\mathcal{T}_p}\nabla\cdot(\boldsymbol{v}_{T'} - \boldsymbol{v}_T)(P). \tag{2.22}$$

It follows from (2.22) that

$$\sum_{P\in\mathcal{V}_T}|\nabla\cdot(\boldsymbol{v}_T - E_h\boldsymbol{v})(P)|^2 \lesssim \sum_{P\in\mathcal{V}_T}\sum_{F\in\mathcal{F}_p}\frac{1}{|e|}\|[\![\nabla\times\boldsymbol{v}]\!]\|^2_{L^2(F)}, \tag{2.23}$$

where $\mathcal{F}_p$ is the set of the faces in $\mathcal{F}_h$ that share the common endpoint P.

Similarly we have

$$\sum_{P\in\mathcal{M}_T} |\nabla\times(\boldsymbol{v}_T - E_h\boldsymbol{v})\times\boldsymbol{n}(P)|^2 \lesssim \sum_{F\in\mathcal{F}_h}\frac{1}{|e|}\|[\![\nabla\times\boldsymbol{v}]\!]\|^2_{L^2(F)}. \tag{2.24}$$

Hence, the estimate (2.18) can be obtained by combining (2.9), (2.20), (2.21), (2.23), (2.24) and summing over all the triangles in $\mathcal{T}_h$. The estimate (2.19) follows from (2.18) and an inverse estimate below:

$$\begin{aligned}|E_h\boldsymbol{v}|^2_{H^2(\Omega)} &\lesssim \sum_{T\in\mathcal{T}_h}|\boldsymbol{v}-E_h\boldsymbol{v}|^2_{H^2(T)} + \sum_{T\in\mathcal{T}_h}|\boldsymbol{v}|^2_{H^2(T)}\\ &\lesssim \sum_{T\in\mathcal{T}_h}\left[h_T^{-4}\|\boldsymbol{v}-E_h\boldsymbol{v}\|^2_{L^2(T)} + \|\nabla\times\nabla\times\boldsymbol{v}\|^2_{L^2(T)}\right] \lesssim |\!|\!|\boldsymbol{v}|\!|\!|^2_{H^2(\Omega,\mathcal{T}_h)}.\end{aligned}$$

□

Corollary 1. We have

$$|E_h\boldsymbol{v}|_{H^2(\Omega)} \lesssim \|\boldsymbol{v}\|_h, \qquad \forall\,\boldsymbol{v}\in V_h. \tag{2.25}$$

Let $\Pi_h : H_0(\mathrm{curl};\Omega)\cap H(\mathrm{div}^0;\Omega)\to V_h$ be the nodal interpolation operator. Since $\Pi_h(E_h\boldsymbol{v})$ and $\boldsymbol{v}$ have identical dofs, it directly follows from the construction of the enriching operator that the following property holds

$$\Pi_h(E_h\boldsymbol{v}) = \boldsymbol{v}, \qquad \forall\,\boldsymbol{v}\in V_h.$$

The following result shows that the composition $E_h\circ\Pi_h$ behaves like a quasi-interpolation operator (cf. [6]).

Lemma 6. *For any $s\geq 2$, there exists a positive constant C depending only on s and the shape regularity of $\mathcal{T}_h$ such that*

$$\sum_{m=0}^{2} h_T^{2m}|\boldsymbol{\xi}-E_h\Pi_h\boldsymbol{\xi}|^2_{H^m(T)} \leq Ch_T^{2s}|\boldsymbol{\xi}|^2_{H^s(S_T)}, \tag{2.26}$$

for all $T\in\mathcal{T}_h$ and $\boldsymbol{\xi}\in[H^s(S_T)]^3\cap[C^0(\overline{\Omega})]^3$, where S_T is the union of the tetrahedrons in $\mathcal{T}_h$ that share a common vertex with T.

3 Convergence analysis

3.1 Error estimates in energy norm

In this section, we derive discretization error estimates for the C^0 interior penalty method introduced in section 2.

The next lemma, which gives the abstract error estimate, is a direct consequence of the (2.5), (2.7) and (2.12).

Lemma 7. *Let $\boldsymbol{u}$ and $\boldsymbol{u}_h$ be the solutions of (1.2) and (2.3), respectively. Then the following estimate holds:*

$$\|\boldsymbol{u}-\boldsymbol{u}_h\|_h \lesssim \inf_{\boldsymbol{v}\in V_h}\|\boldsymbol{u}-\boldsymbol{v}\|_h.$$

By the definition of Π_h, we have the standard interpolation error estimate (cf. [6]):

$$\sum_{m=0}^{2} h_T^{2m}|\boldsymbol{\xi}-\Pi_h\boldsymbol{\xi}|^2_{H^m(T)} \le Ch_T^{2\gamma}|\boldsymbol{\xi}|^2_{H^s(T)}, \tag{3.1}$$

for all $T\in\mathcal{T}_h$ and $\boldsymbol{\xi}\in[H^s(T)]^3\cap[C^0(\overline{\Omega})]^3$, where $\gamma=\min(s,k+1)$.

Lemma 8. *Let $\boldsymbol{u}\in\mathbb{E}$ be the solution of problem (1.2), and assume $\boldsymbol{u}\in[H^{2+\alpha}(\Omega)]^3$, $\frac{1}{2}<\alpha\le 1$. Then the following interpolation error estimate hold:*

$$\|\boldsymbol{u}-\Pi_h\boldsymbol{u}\|_h \lesssim h^{\alpha}|\boldsymbol{u}|_{H^{2+\alpha}(\Omega)}. \tag{3.2}$$

Proof. According to (2.6), we have

$$\begin{aligned}\|\boldsymbol{u}-\Pi_h\boldsymbol{u}\|_h^2 =& \sum_{T\in\mathcal{T}_h}\|\nabla\times\nabla\times(\boldsymbol{u}-\Pi_h\boldsymbol{u})\|^2_{L^2(T)} + \sum_{T\in\mathcal{T}_h}\|\nabla\times(\boldsymbol{u}-\Pi_h\boldsymbol{u})\|^2_{L^2(T)}\\ &+\sum_{T\in\mathcal{T}_h}\|\boldsymbol{u}-\Pi_h\boldsymbol{u}\|^2_{L^2(T)} + \sum_{F\in\mathcal{F}_h}\frac{1}{|e|}\|[\![\nabla\times(\boldsymbol{u}-\Pi_h\boldsymbol{u})]\!]\|^2_{L^2(F)}\\ &+\sum_{F\in\mathcal{F}}|e|\|\{\!\{\nabla\times\nabla\times(\boldsymbol{u}-\Pi_h\boldsymbol{u})\}\!\}\|^2_{L^2(F)} + \sum_{T\in\mathcal{T}_h}\frac{1}{h_T^2}\|\nabla\cdot(\boldsymbol{u}-\Pi_h\boldsymbol{u})\|^2_{L^2(T)}.\end{aligned} \tag{3.3}$$

It follows from (3.1) that

$$\begin{aligned}\|\nabla\times\nabla\times(\boldsymbol{u}-\Pi_h\boldsymbol{u})\|^2_{L^2(T)} &\le |\boldsymbol{u}-\Pi_h\boldsymbol{u}|^2_{H^2(T)} \lesssim h^{2\alpha}|\boldsymbol{u}|^2_{H^{2+\alpha}(T)},\\ \|\nabla\times(\boldsymbol{u}-\Pi_h\boldsymbol{u})\|^2_{L^2(T)} &\le |\boldsymbol{u}-\Pi_h\boldsymbol{u}|^2_{H^1(T)} \lesssim h^{2\alpha+2}|\boldsymbol{u}|^2_{H^{2+\alpha}(T)},\\ \|\boldsymbol{u}-\Pi_h\boldsymbol{u}\|^2_{L^2(T)} &\lesssim h^{2\alpha+4}|\boldsymbol{u}|^2_{H^{2+\alpha}(T)},\\ \frac{1}{h_T^2}\|\nabla\cdot(\boldsymbol{u}-\Pi_h\boldsymbol{u})\|^2_{L^2(T)} &\le h_T^{-2}|\boldsymbol{u}-\Pi_h\boldsymbol{u}|^2_{H^1(T)} \lesssim h^{2\alpha}|\boldsymbol{u}|^2_{H^{2+\alpha}(T)}.\end{aligned} \tag{3.4}$$

By using trace theory with scaling and standard interpolation error estimate, we have

$$\begin{aligned}&\sum_{F\in\mathcal{F}_h}|e|^{-1}\|[\![\nabla\times(\boldsymbol{u}-\Pi_h\boldsymbol{u})]\!]\|^2_{L^2(F)} \le \sum_{F\in\mathcal{F}_h}|e|^{-1}\|\nabla\times(\boldsymbol{u}-\Pi_h\boldsymbol{u})\|^2_{L^2(F)}\\ &\lesssim \sum_{T\in\mathcal{T}_h}h^{-2}|\boldsymbol{u}-\Pi_h\boldsymbol{u}|^2_{H^1(T)} + |\boldsymbol{u}-\Pi_h\boldsymbol{u}|^2_{H^2(T)} \lesssim \sum_{T\in\mathcal{T}_h}h^{2\alpha}|\boldsymbol{u}|^2_{H^{2+\alpha}(T)}.\end{aligned}$$

It follows from (2.10) and (3.4) that

$$\begin{aligned}\sum_{F\in\mathcal{F}_h}|e|\|\{\!\{\nabla\times\nabla\times(\boldsymbol{u}-\Pi_h\boldsymbol{u})\}\!\}\|^2_{L^2(F)} &\le \sum_{T\in\mathcal{T}_h}\|\nabla\times\nabla\times(\boldsymbol{u}-\Pi_h\boldsymbol{u})\|^2_{L^2(T)}\\ &\lesssim h^{2\alpha}|\boldsymbol{u}|^2_{H^{2+\alpha}(T)}.\end{aligned} \tag{3.5}$$

Finally, the interpolation error estimate (3.2) holds by combining (3.3)–(3.5). □

The error estimate for the C^0-IP method is given in the following theorem, which directly follows from Lemma 7 and Lemma 8.

Theorem 1. *Let $\boldsymbol{u}$ be the solution of problem (1.2), assume $\boldsymbol{u} \in [H^{2+\alpha}(\Omega)]^3$. Suppose $\boldsymbol{u}_h$ is the solution of the discrete variational problem (2.3), then we have*

$$\|\boldsymbol{u} - \boldsymbol{u}_h\|_h \lesssim h^{\alpha} |\boldsymbol{u}|_{H^{2+\alpha}(\Omega)}. \tag{3.6}$$

3.2 Error estimate in a lower order norm

Now we investigate the discretization error in lower order norms for C^0 interior penalty method.

Lemma 9. *Let $\boldsymbol{u}$ be the exact solution, $\boldsymbol{u}_h \in V_h$ be the solution of C^0-IP method and define $F = \int_\Omega \boldsymbol{f} \cdot \boldsymbol{v} dx$, $\forall\, v \in \mathbb{E}$. Assume $\boldsymbol{u} \in [H^{2+\alpha}(\Omega)]^2$. Then we have*

$$\|\boldsymbol{u} - \boldsymbol{u}_h\|_{H^{2-\alpha}(\Omega)} \lesssim h^{2\alpha} \|F\|_{H^{-2+\alpha}(\Omega)}. \tag{3.7}$$

Proof. Let $G \in [H^{-2+\alpha}(\Omega)]^2$ be arbitrary and $\xi \in [H^{2+\alpha}(\Omega)]^3$ be defined by $a(\xi, \boldsymbol{v}) = G(\boldsymbol{v})$, $\forall\, \boldsymbol{v} \in \mathbb{E}$. Then we have by shifting theory and comparing (1.3) and (2.4) that

$$\begin{aligned} &\|\xi\|_{H^{2+\alpha}(\Omega)} \lesssim \|G\|_{H^{-2+\alpha}(\Omega)}, \\ &a_h(\xi, \boldsymbol{v}) = G(\boldsymbol{v}), \quad \forall\, \boldsymbol{v} \in V_h. \end{aligned} \tag{3.8}$$

Then we have by (2.5), (2.7), (3.2), (3.6) and (3.8) that

$$\begin{aligned} &G(\boldsymbol{u} - \boldsymbol{u}_h) = a_h(\xi, \boldsymbol{u} - \boldsymbol{u}_h) = a_h(\xi - \Pi_h \xi, \boldsymbol{u} - \boldsymbol{u}_h) \\ &\lesssim \|\xi - \Pi_h \xi\|_h \|\boldsymbol{u} - \boldsymbol{u}_h\|_h \lesssim h^{2\alpha} \|G\|_{H^{-2+\alpha}(\Omega)} \|F\|_{H^{-2+\alpha}(\Omega)}. \end{aligned} \tag{3.9}$$

Also, we have the duality formula

$$\|\boldsymbol{w}\|_{H^{2-\alpha}(\Omega)} = \sup_{\substack{G \in [H^{-2+\alpha}(\Omega)]^3 \\ G \neq 0}} \frac{G(\boldsymbol{w})}{\|G\|_{H^{-2+\alpha}(\Omega)}}, \quad \forall \boldsymbol{w} \in [H^{2-\alpha}(\Omega)]^3. \tag{3.10}$$

The estimate (3.7) follows from (3.9) and (3.10). □

3.3 Post-processing

Let $E_h : V_h \to [H_0^2(\Omega)]^3$ be the enriching operator introduced in subsection 2.4. The C^1 finite element function $E_h \boldsymbol{u}_h$ obtained by post-processing provides an (smooth) approximation of $\boldsymbol{u}$ in the space W_h. Recall that S_T is the union of polyhedrons in $\mathcal{T}_h$ that share a common vertex with T, and note that $\boldsymbol{u} \in H^{2+\alpha(S_T)}(S_T)$, where

$$\alpha(S_T) = \min_{T' \in S_T} \alpha(T').$$

The error estimate for $E_h \boldsymbol{u}_h$ is given in the next theorem.

Theorem 2. *Under the assumptions of Theorem 1, we have*

$$|\boldsymbol{u} - E_h\boldsymbol{u}_h|_{H^2(\Omega)} \leq C\Big[\sum_{T\in\mathcal{T}_h} h_T^{2min(\alpha(S_T),k-1)}|\boldsymbol{u}|^2_{H^{2+\alpha(S_T)}(S_T)}\Big]^{\frac{1}{2}}, \tag{3.11}$$

where α is the index of elliptic regularity and the positive constant C depends only on the shape regularity of $\mathcal{T}_h$.

Proof. From (2.25) we have

$$\begin{aligned}|\boldsymbol{u} - E_h\boldsymbol{u}_h|_{H^2(\Omega)} &\leq |\boldsymbol{u} - E_h\Pi_h\boldsymbol{u}|_{H^2(\Omega)} + |E_h(\Pi_h\boldsymbol{u} - \boldsymbol{u}_h)|_{H^2(\Omega)}\\ &\leq |\boldsymbol{u} - E_h\Pi_h\boldsymbol{u}|_{H^2(\Omega)} + \|\Pi_h\boldsymbol{u} - \boldsymbol{u}\|_h + \|\boldsymbol{u} - \boldsymbol{u}_h\|_h. \end{aligned}\tag{3.12}$$

The estimate (3.11) then follows from (2.26), (3.1), (3.6) and (3.12). □

4 Numerical results

In this section we report the results of numerical experiments in two dimensions. All three numerical experiments are carried out on quasi-uniform triangulations. We take α and β both to be 1. Besides the errors in the energy norm and L^∞ norm, we also include the errors in the norm $\|\cdot\|_{H(\mathrm{curl},\Omega)}$ which is defined by

$$\|\boldsymbol{u}\|_{H(\mathrm{curl},\Omega)} = \|\nabla\times\boldsymbol{u}\|_{L^2(\Omega)}.$$

Experiment 4.1. In the first experiment we take the exact solution $\boldsymbol{u} = \nabla\times\phi$ where

$$\phi(x) = \sin^3(\pi x_1)\sin^3(\pi x_2).$$

Note that the choice of ϕ ensures that $\boldsymbol{u}\in\mathbb{E}$. The domain for this experiment is $[0,1]^2$. The relative errors are reported in Table 1. The results show that the

Table 1. Results for the C^0 interior penalty method for Experiment 4.1.

h	$\frac{\|\boldsymbol{u}-\boldsymbol{u}_h\|_h}{\|\boldsymbol{u}\|_h}$	Order	$\frac{\|\nabla\times\boldsymbol{u}-\nabla\times\boldsymbol{u}_h\|_{H(\mathrm{curl},\Omega)}}{\|\nabla\times\boldsymbol{u}\|_{H(\mathrm{curl},\Omega)}}$	Order	$\frac{\|\boldsymbol{u}-E_h\boldsymbol{u}_h\|_{H^2(\Omega)}}{\|\boldsymbol{u}\|_{H^2(\Omega)}}$	Order
1	2.4910E−01	–	1.6237E−00	–	1.6097E−00	–
1/2	5.6200E−02	2.1484	2.8650E−01	2.5027	2.8540E−01	2.4956
1/4	7.7500E−02	-0.4639	3.1480E−01	-0.1358	3.1490E−01	-0.1419
1/8	5.9000E−02	0.3940	1.6940E−01	0.8935	1.6990E−01	0.8903
1/16	3.5300E−02	0.7404	6.5900E−02	1.3624	6.6100E−02	1.3612
1/32	1.7600E−02	1.0008	2.0500E−02	1.6855	2.0600E−02	1.6849
1/64	9.1000E−03	0.9484	5.8000E−03	1.8321	5.8000E−03	1.8318

errors obtained by the C^0-IP scheme (2.3) have first order convergence rate in the energy norm. Furthermore, the scheme has nearly second order convergence in the $\|\cdot\|_{H(\mathrm{curl},\Omega)}$ norm. This super-convergence behavior may due to the fact that exact solution $\boldsymbol{u}$ is very smooth in this case. We also present the the convergent result for the enriched solution $E_h\boldsymbol{u}_h$ in the H^2 norm in this table. We see that the enriched solution $E_h\boldsymbol{u}_h$ converge to the exact solution in a second order of h in H^2 norm, which verifies the theoretical analysis.

In [23], we also studied a mixed finite element method for this example. In order to provide a comparison in terms of efficiency, we plot the convergent error of $\|\boldsymbol{u}-\boldsymbol{u}_h\|_{H(\mathrm{curl},\Omega)}/\|\boldsymbol{u}\|_{H(\mathrm{curl},\Omega)}$ with computational time for the C^0-IP method and the mixed method in Figure 2. We observe that the C^0-IP method takes less time than the mixed finite element method in order to achieve the same accuracy.

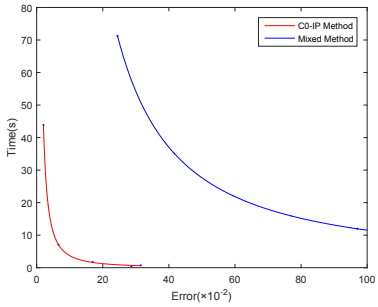

Figure 2. Computational time for C^0-IP method and mixed method for Experiment 1.

We notice that this example was also studied by Brenner et al. in [5] by using Hodge decomposition method. We give a comparison of accuracy for $\|\boldsymbol{u}-\boldsymbol{u}_h\|_{L^2(\Omega)}$ with degree of freedoms (DOFs) in Table 2. We see that C^0-IP method method takes less DOFs to achieve a higher accuracy for the P_1 case. The accuracy for Hodge decomposition using P_2 Lagrange finite element method is better than C^0-IP method at the cost of more DOFs.

Table 2. DOFs required for achieved error of $\|\boldsymbol{u}-\boldsymbol{u}_h\|_{L^2(\Omega)}$ for Experiment 1.

h	C^0-IP method		Hodge decomposition method (P_1)		Hodge decomposition method (P_2)	
	$\|\boldsymbol{u}-\boldsymbol{u}_h\|_{L^2(\Omega)}$	DOFs	$\|\boldsymbol{u}-\boldsymbol{u}_h\|_{L^2(\Omega)}$	DOFs	$\|\boldsymbol{u}-\boldsymbol{u}_h\|_{L^2(\Omega)}$	DOFs
1/10	8.9890E−01	25	3.58137E−01	1.200E02	3.09934E−02	3.600E02
1/20	5.7500E−01	81	1.68292E−01	4.800E02	7.85594E−03	1.440E03
1/40	2.0510E−01	289	8.25728E−02	1.920E03	1.97684E−03	5.760E03
1/80	6.0900E−02	1089	4.10892E−02	7.680E03	4.95696E−04	2.304E04
1/160	1.6200E−02	4225	2.05210E−02	3.072E04	1.24101E−04	9.216E04

Experiment 4.2. In the second experiment we take a piecewise constant vector field $\boldsymbol{f}$ defined by

$$\boldsymbol{f}=\begin{cases}[0,\quad 1]^T, & x_1+x_2<1,\\ [1,\quad 0]^T, & x_1+x_2\geq 1,\end{cases}$$

to be the right-hand side function of (1.2). We take $\Omega=[0,1]^2$ in this experiment. Since the exact solution is not available in this case, we use the differences of numerical solutions on consecutive levels to measure the errors. The relative errors are reported in Table 3. The errors converge with the first order rate in both the energy norm and the $\|\cdot\|_{H(\mathrm{curl},\Omega)}$ norm, which agree with the theoretical results.

Table 3. Results for the C^0 interior penalty method for Experiment 4.2.

h	$\frac{\|\boldsymbol{u}_h^i-\boldsymbol{u}_h^{i+1}\|_h}{\|\boldsymbol{u}_h^{i+1}\|_h}$	Order	$\frac{\|\nabla\times\boldsymbol{u}_h^i-\nabla\times\boldsymbol{u}_h^{i+1}\|_{H(\mathrm{Curl},\Omega)}}{\|\nabla\times\boldsymbol{u}_h^{i+1}\|_{H(\mathrm{Curl},\Omega)}}$	Order	$\frac{\|\boldsymbol{u}_h^i-\boldsymbol{u}_h^{i+1}\|_{L^\infty(\Omega)}}{\|\boldsymbol{u}_h^{i+1}\|_{L^\infty(\Omega)}}$	Order
1/2	7.1394E−00	–	5.1867E−00	–	3.6957E−00	–
1/4	9.0100E−01	2.9863	8.5540E−01	2.6002	3.4100E−01	3.4381
1/8	4.9670E−01	0.8591	5.2940E−01	0.6921	2.4310E−01	0.4884
1/16	2.6580E−01	0.9021	2.9590E−01	0.8395	9.1500E−02	1.4096
1/32	1.3460E−01	0.9813	1.5410E−01	0.9410	2.8500E−02	1.6843
1/64	6.7100E−02	1.0041	7.8200E−02	0.9792	1.0000E−02	1.5147

Experiment 4.3. In the third experiment we consider a non-simply connected domain $\Omega = [(0,4)\times(0,4)]\backslash[(1,3)\times(1,3)]$. The exact solution is taken to be $\boldsymbol{u} = \nabla\times\phi$, where $\phi(x) = \sin^3(4\pi x_1)\sin^3(4\pi x_2)$. In this case,

$$\boldsymbol{u} = \nabla\times\phi = \begin{bmatrix} \frac{\partial\phi}{\partial x_2} \\ -\frac{\partial\phi}{\partial x_1} \end{bmatrix} = \begin{bmatrix} 12\pi\sin^3(4\pi x_1)\cos(4\pi x_2)\sin^2(4\pi x_2) \\ -12\pi\cos(4\pi x_1)\sin^2(4\pi x_1)\sin^3(4\pi x_2) \end{bmatrix}.$$

Then we have

$$\begin{aligned}\nabla\times\boldsymbol{u} = -96\pi^2\sin(4\pi)\sin(4\pi x_2)\big(&-3\sin^2(4\pi x_1)\sin^2(4\pi x_2)\\ &+\sin^2(4\pi x_1)+\sin^2(4\pi x_2)\big)\end{aligned}$$

and $\nabla\times\boldsymbol{u} = 0$ on $\partial\Omega$. It is obviously that $\boldsymbol{u}\in\mathbb{E}$ since $\nabla\cdot\boldsymbol{u} = 0$, and $\boldsymbol{n}\times\boldsymbol{u} = 0$ on $\partial\Omega$. We depict the second components of the (enriched) numerical solution $E_h\boldsymbol{u}_h$ on consecutive levels in Figure 3 and that of the exact solution on final level in Figure 5, i.e., the nodal values of exact solution on the mesh with $h = 1/64$ are depicted. We also present the second components of numerical solution $\boldsymbol{u}_h$ obtained by C^0-IP method in Figure 4. It can be observed that the post-processed numerical solutions are C^1 smooth and quickly converge to the true solution.

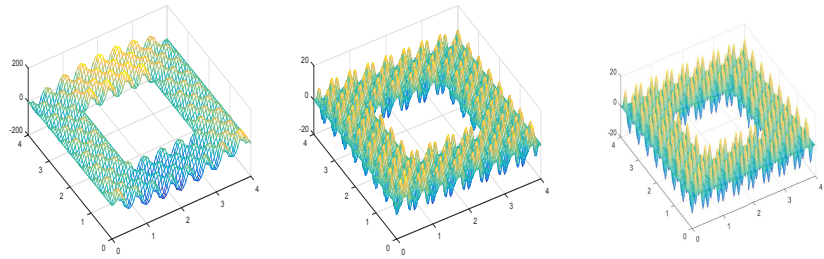

(a) (b) (c)

Figure 3. Post-processed (enriched) solution u_2 for (a) $h = 1/16$; (b) $h = 1/32$; (c) $h = 1/64$.

In [21], we studied multigrid fast solvers based on the C^0-IP method. In that paper, we test W-cycle multigrid algorithm for the same numerical example. We present the errors and computational time on each level in Table 4. Here $\boldsymbol{u}_h^{MG}$ is the numerical solution obtained by multigrid method. We see that

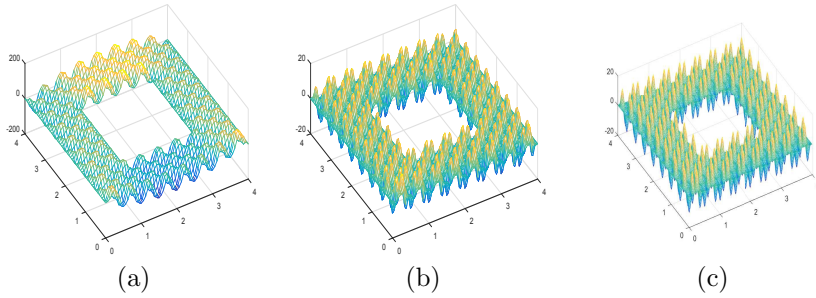

Figure 4. Numerical solution u_2 for (a) $h = 1/16$; (b) $h = 1/32$; (c) $h = 1/64$.

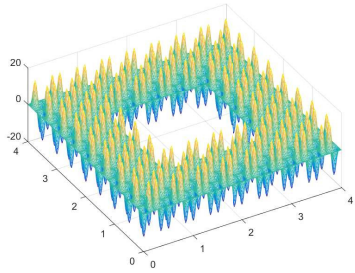

Figure 5. Exact solution u_2 for $h = 1/64$.

the computation time is greatly reduced by using multigrid method on higher levels, while the errors remain the same order of accuracy.

Table 4. The computational time for Experiment 4.3.

h	$\frac{\|\boldsymbol{u}-E_h\boldsymbol{u}_h\|_h}{\|\boldsymbol{u}\|_h}$	Time(s)	$\frac{\|\boldsymbol{u}-\boldsymbol{u}_h^{MG}\|_h}{\|\boldsymbol{u}\|_h}$	Time(s)
1/8	1.2295E−00	1.23	1.2239E−00	5.28
1/16	3.9910E−01	7.99	5.0140E−01	15.37
1/32	1.9850E−01	79.84	3.8250E−01	418.23
1/64	1.1341E−01	10690.05	2.3590E−01	6486.92

5 Conclusions

In this paper, we developed the C^0 interior penalty method for solving the quad-curl problem which arises in the MHD model. We established the well-posedness of the numerical scheme, in which we weakly enforce the divergence-free condition by adding an extra penalty term. Optimal convergence rates are proved on convex polyhedral/polygonal domains based on uniform meshes. We further constructed an enriching operator for the numerical solution in three dimensions. It provides an approximation of $\boldsymbol{u}$ in the C^1-Ženíšek finite element space and also preserves the convergence property of C^0 interior penalty method.

We would be able to further improve the convergence rate of the new C^0-IP method on nonconvex domains by using graded meshes [3]. The grading strategy will be closely related to the elliptic regularity of the fourth-order model problem. Moreover, we would like to study the *a posteriori* error estimate for the C^0-IP method and its fast solvers. Those will all be carried out in our future work.

Acknowledgements

The first two authors are co-first authors as they contributed equally to this work. The authors' research are supported in part by National Natural Science Foundation of China (NSFC) no. 11771367, 11871038, China Postdoctoral Science Foundation no. 2014M560547, and Shenzhen University Research Grant 85202-00000538.

References

[1] D. Biskamp. *Magnetic reconnection in plasmas*. Number 3. Cambridge University Press, 2005.

[2] S.C. Brenner. C^0 interior penalty methods. In *Frontiers in Numerical Analysis-Durham 2010*, pp. 79–147. Springer, 2011. https://doi.org/10.1007/978-3-642-23914-4_2.

[3] S.C. Brenner, J. Cui, T. Gudi and L.-Y. Sung. Multigrid algorithms for symmetric discontinuous Galerkin methods on graded meshes. *Numerische Mathematik*, **119**(1):21–47, 2011. https://doi.org/0.1007/s00211-011-0379-y.

[4] S.C. Brenner and R. Scott. *The mathematical theory of finite element methods*, volume 15. Springer Science and Business Media, 2007.

[5] S.C. Brenner, J. Sun and L.-Y. Sung. Hodge decomposition methods for a quad-curl problem on planar domains. *Journal of Scientific Computing*, **73**(2):495–513, 2017. https://doi.org/10.1007/s10915-017-0449-0.

[6] S.C. Brenner and L.-Y. Sung. C^0 interior penalty methods for fourth order elliptic boundary value problems on polygonal domains. *Journal of Scientific Computing*, **22**(1-3):83–118, 2005. https://doi.org/10.1007/s10915-004-4135-7.

[7] S.C. Brenner and L.-Y. Sung. Multigrid algorithms for C^0 interior penalty methods. *SIAM Journal on Numerical Analysis*, **44**(1):199–223, 2006. https://doi.org/10.1137/040611835.

[8] S.C. Brenner, L.-Y. Sung, H. Zhang and Y. Zhang. A quadratic C^0 interior penalty method for the displacement obstacle problem of clamped Kirchhoff plates. *SIAM Journal on Numerical Analysis*, **50**(6):3329–3350, 2012. https://doi.org/10.1137/110845926.

[9] F. Cakoni, D. Colton, P. Monk and J. Sun. The inverse electromagnetic scattering problem for anisotropic media. *Inverse Problems*, **26**(7):074004, 2010. https://doi.org/10.1088/0266-5611/26/7/074004.

[10] F. Cakoni and H. Haddar. A variational approach for the solution of the electromagnetic interior transmission problem for anisotropic media. *Inverse Problems and Imaging*, **1**(3):443–456, 2007. https://doi.org/10.3934/ipi.2007.1.443.

[11] L. Chacón, A.N. Simakov and A. Zocco. Steady-state properties of driven magnetic reconnection in 2D electron magnetohydrodynamics. *Physical Review Letters*, **99**(23):235001, 2007. https://doi.org/10.1103/PhysRevLett.99.235001.

[12] G. Chen, W. Qiu and L. Xu. Analysis of a mixed finite element method for the quad-curl problem. *arXiv preprint arXiv:1811.06724*, 2018.

[13] Q. Hong, J. Hu, S. Shu and J. Xu. A discontinuous Galerkin method for the fourth-order curl problem. *Journal of Computational Mathematics*, **30**(6):565–578, 2012. https://doi.org/10.4208/jcm.1206-m3572.

[14] W. Ming and J. Xu. The Morley element for fourth order elliptic equations in any dimensions. *Numerische Mathematik*, **103**(1):155–169, 2006. https://doi.org/10.1007/s00211-005-0662-x.

[15] P. Monk and J. Sun. Finite element methods for Maxwell's transmission eigenvalues. *SIAM Journal on Scientific Computing*, **34**(3):B247–B264, 2012. https://doi.org/10.1137/110839990.

[16] L.S.D. Morley. The triangular equilibrium element in the solution of plate bending problems. *The Aeronautical Quarterly*, **19**(2):149–169, 1968. https://doi.org/10.1017/S0001925900004546.

[17] J.-C. Nédélec. Mixed finite elements in R^3. *Numerische Mathematik*, **35**(3):315–341, 1980. https://doi.org/10.1007/BF01396415.

[18] J.-C. Nédélec. A new family of mixed finite elements in R^3. *Numerische Mathematik*, **50**(1):57–81, 1986. https://doi.org/10.1007/BF01389668.

[19] S. Nicaise. Singularities of the quad curl problem. *Journal of Differential Equations*, **264**(8):5025–5069, 2018. https://doi.org/10.1016/j.jde.2017.12.032.

[20] J. Sun. A mixed FEM for the quad-curl eigenvalue problem. *Numerische Mathematik*, **132**(1):185–200, 2016. https://doi.org/10.1007/s00211-015-0708-7.

[21] Z. Sun, J. Cui, F. Gao and C. Wang. Multigrid methods for a quad-curl problem based on C^0 interior penalty method. *Computers & Mathematics with Applications*, **76**(9):2192–2211, 2018. https://doi.org/10.1016/j.camwa.2018.07.048.

[22] Alexander Ženíšek. Tetrahedral finite C^m-elements. *Acta Universitatis Carolinae. Mathematica et Physica*, **15**(1):189–193, 1974.

[23] C. Wang, Z. Sun and J. Cui. A new error analysis of a mixed finite element method for the quad-curl problem. *Applied Mathematics and Computation*, **349**:23–38, 2019. https://doi.org/10.1016/j.amc.2018.12.027.

[24] Q. Zhang, L. Wang and Z. Zhang. An H^2(curl)-conforming finite element in 2D and its applications to the quad-curl problem. *SIAM Journal on Scientific Computing*, **41**(3):A1527–A1547, 2019. https://doi.org/10.1137/18M1199988.

[25] S. Zhang. Mixed schemes for quad-curl equations. *ESAIM: Mathematical Modelling and Numerical Analysis*, **52**(1):147–161, 2018. https://doi.org/10.1051/m2an/2018005.

[26] B. Zheng, Q. Hu and J. Xu. A nonconforming finite element method for fourth order curl equations in R^3. *Mathematics of Computation*, **80**(276):1871–1886, 2011. https://doi.org/10.1090/S0025-5718-2011-02480-4.